The final version of this article was published in

Journal of Sol-Gel Science and Technology

59(2) 327-333 (2011)

DOI: 10.1007/s10971-011-2505-9

Optical and structural properties of aluminium oxide thin films prepared by a non-aqueous sol-gel technique

[1]Avci Nursen, [1]Smet Philippe F., [2]Lauwaert Johan, [2]Vrielinck Henk, [1]Poelman Dirk

[1]LumiLab, Department of Solid State Sciences, Ghent University, Krijgslaan 281-S1, B-9000 Gent/Belgium

[2]Defects in Semiconductors, Department of Solid State Sciences, Ghent University, Krijgslaan 281-S1, B-9000 Gent/Belgium

Corresponding author: Tel: +329 / 264 45 77

Fax: +329 / 264 49 96

Email address: Nursen.Avci@UGent.be

URL: http://LumiLab.ugent.be/

Abstract

Clear aluminium oxide sols without precipitation were synthesized via a non-aqueous sol-gel technique using three different alcohols (ethanol, isopropanol and n-butyl alcohol) as solvent, aluminium sec-butoxide as a precursor and acetyl acetone as a chelating agent. Although all sols could be successfully used to prepare thin films, the most stable one was prepared with n-butyl alcohol. Highly transparent, homogenous and amorphous aluminium oxide thin films were obtained on Si substrates after a heat treatment at 500^{o}C. X-ray photoelectron spectroscopy (XPS) and Fourier transform infrared absorption (FT-IR) spectroscopy revealed all

films were hydroxide free. The optical and structural properties of the films were particularly investigated. Any significant difference except from thickness on the film properties was not observed by changing the alcohol. Refractive index was used as an indication of the porosity of the films and ranged from 1.54 to 1.60.

.

Keyword: *Aluminium oxide; non-aqueous sol-gel; thin film; optical properties****.***

Introduction

Aluminium oxide is a versatile and technologically important material because of its wide transparency window from ultra-violet to mid-infrared [1-3], good thermal and chemical stability [4, 5], and superior electrical and mechanical properties [6, 7].

Especially aluminium oxide in thin film form has a broad application range including use as water-repellent coating [8, 9], dielectric [6] and sensing layer [10] and optical [11] and protective coating [1, 12-15]. These application areas make synthesis and characterization of aluminium oxide films attractive. To synthesize aluminium oxide films several techniques have been used such as atomic layer deposition (ALD) [1, 14, 15], electron beam deposition [11], magnetron sputtering [16], chemical vapor deposition (CVD) [17] and pulsed laser deposition (PLD) [18]. These techniques have one or more of the following disadvantages: difficulty in controlling the stoichiometry, long deposition times and high costs for fabrication. As an alternative approach the sol-gel technique overcomes these problems because it puts forward excellent control of stoichiometry, density and microstructure. Moreover, large areas can be coated using simple equipment without the need for vacuum. Therefore the fabrication is relatively low cost.

Although aqueous sol-gel is a very useful technique to prepare a homogeneous aluminium oxide layer, in some cases such as rare-earth doped layers and protection layers, there are a few drawbacks in this method. Er^{3+} doped Al_2O_3 is a well known material as planar waveguide; Al_2O_3 improves the dispersion of Er^{3+}, thus the luminescence efficiency and decay time increase. However, using water during the preparation encourages hydrolysis of Er^{3+} and accordingly dispensability of Er^{3+} decreases [4, 10]. Alkaline earth sulfide phosphors are very attractive for different areas such as display applications, electroluminescent devices and optical information storage. In addition, they are considered as very promising material for wavelength converter in light emitting diodes (LEDs) [19]. Notwithstanding, because of the limited stability with respect to water and other atmospheric

components, it is not obvious to use sulfides as phosphor hosts. This problem can be solved via encapsulation with an inert film like Al_2O_3 [1, 20]. Porosity, stability, homogeneity and transparency determine the efficiency of such a layer.

For both applications, the presence of water added into the solution for hydrolysis reaction is to be avoided. In addition, using a strong acid as a dispersing agent to prepare protection layers may be detrimental to both sulfide particles and substrate surface. Thus, coatings based on these kinds of solution may provide degradation rather than protection. The problem can be overcome using non-aqueous sol-gel techniques [20].

In this study we synthesized amorphous aluminium oxide films using three different alcohols as a solvent via a non-aqueous sol-gel technique. The utility of the alumina layer when used as protective coating for luminescent particles is affected by the structural properties, such as the crystallinity and the porosity. A high transparency of the coating layer for the excitation and emission wavelengths of the luminescent particles is of prime importance to avoid absorption losses due to the coating. Finally, a low synthesis temperature for the protective layer is favourable to limit possible degradation of the luminescent particles during the heat treatment. The protective properties of the resulting Al_2O_3 layers have been published elsewhere [20]. Hence this paper focuses on the structural and the optical properties of the alumina films, as a function of heating temperature.

Experimental

Aluminium oxide films were prepared via a non-aqueous sol-gel technique. Three sols were synthesized using anhydrous ethanol (EtOH) (Alfa Aesar, 90%), isopropanol (Pr^iOH) (Acros, 99.5%) and n-butyl alcohol (n-BuOH) (Alfa Aesar, 99.4%) as solvent. Aluminium sec-butoxide ($Al[O(CH_3)CHC_2H_5]_3$) (Alfa Aesar, 95%) was used as a precursor. Acetylacetone (AcAcH) (Alfa Aesar, 99%) was added as chelating agent to decrease the reactivity of the precursor. The molar ratio between acetylacetone and aluminium sec-butoxide was 1. The concentration of the sols was adjusted to 0.5 M. To prepare stable sols, first the solvent and acetylacetone were mixed, and then aluminium sec-butoxide was added to this mixture. Eventually the solution was stirred for 6 hours at 30^{o}C. Transparent solutions were readily obtained using Pr^iOH and n-BuOH as solvent via this route. To obtain a

transparent solution using EtOH as a solvent, it was necessary to stir at 40^{o}C. The sol prepared with n-BuOH was stable for more than 1 year while the sols prepared with EtOH and Pr^{i}OH were stable for 1 and 8 months, respectively, after which precipitation occurred.

Single aluminium oxide layers were deposited on (100)-oriented silicon wafers by spin coating with different spinning rate from 1000 to 6000 rpm for 20 seconds at room temperature. Coated substrates were heat treated at 450 and 650^{o}C in air for 30 minutes and the heating rate was 10^{o}C/min. The layers for IR measurement were deposited on double side polished and (100)-oriented Czochralski-grown silicon wafers by spin coating with a spinning rate of 2000 rpm for 20 seconds at room temperature. After the coating process, samples were heat treated at different temperature from 200^{o}C to 500^{o}C in air for 30 minutes and the heating rate was 10^{o}C/min. Aluminium oxide layers for transparency measurements were also prepared by spin coating on corning 1737 sodium-free borosilicate glass substrate at 2000 rpm for 20 seconds at room temperature and then heat treated at 500^{o}C in air for 30 minutes (heating rate of 10^{o}C/min). Thermal Gravimetry Analysis (TGA) and Differential Thermal Analysis (DTA) of the sols were carried out using a SDT 2960 – TA instrument. The measurements were done at a heating rate of 10^{o}C/min from room temperature to 700^{o}C in a flowing air environment. X-ray diffraction (XRD, Bruker D8-Discovery, Cu-Kα radiation) measurements were employed to get information about the crystal structure of the coated layers. Scanning electron microscopy (SEM, FEI Quanta 200 F) was used to characterize the surface morphology. The influence of solvent, spin speed and heat treatment temperature on film thickness and refractive index was determined via spectroscopic ellipsometry (SE, J.A. Woollam Co. Inc., M-2000FI) at an angle of incidence of 65^{o}. The Cauchy dispersion model was used to fit the optical constants; a model including surface roughness of the aluminium oxide films was chosen. Porosity of the films was calculated using the Bruggeman effective medium equation [21]. Transparency measurements of the aluminium oxide thin films on corning 1737 sodium-free borosilicate glass substrate were executed by means of Cary 500 UV-Vis-NIR spectrophotometer. The chemical composition of the films was investigated with X-ray photoelectron spectroscopy (XPS). The base pressure of the chamber was 2x10^{-9} mbar. The spectra were run on an S-Probe XPS spectrometer from Surface Science Instruments (VG) using monochromatic Al-Kα radiation (1486.6 eV). The angle between axis of detector and the sample was 45^{o}. The X-ray source was operated at 10 kV, 200 W. Spectra were acquired at 157.7 eV pass energy with a resolution of 0.15 eV. Depth profiles were carried out by Ar^{+} sputtering at 4 keV with an argon partial

pressure of $1.5x10^{-7}$ mbar and a spot size of 16 mm^2. To avoid artifacts caused by charging of the insulating samples, a charge neutralizer (1 eV) was utilized and the peak positions were calibrated on the C_{1s} peak at 284.6 eV. To identify layer components FT- IR spectroscopy was utilized, the spectra were recorded from 400 to 4000 cm^{-1} with a Bruker IFS66V spectrometer. The resolution was 3 cm^{-1}, and 600 scans were used for every sample. The background spectra were recorded using uncoated double side polished Si substrate.

Results and Discussion

To find the optimum heat treatment temperature for amorphous aluminium oxide, TGA and DTA were performed. Figure 1 shows the TGA and DTA results of three aluminium oxide sols prepared with EtOH, Pr^iOH and n-BuOH.

The TGA and DTA results of the three sols are quite similar. In the TGA curves, two main weight loss stages are observed, in the range from 35 to 200^oC and 200 to 500^oC (fig.1). The first weight loss is induced by evaporation of water and thermal decomposition of the organics. The second one is correlated with the loss of carbon groups in the structure [22]. The weight loss during the dehydroxylation is very low as compared with the weight loss during the evaporation of water and the decomposition of organics [23]. Therefore it is not entirely clear from these measurements whether hydroxides are still present after the heat treatment. Consequently, other analytical techniques, such as XPS and FTIR, were applied to evaluate whether pure alumina thin films, without hydroxides, were obtained after heat treatment.

In case of characterization of the amorphous materials, XPS can be very useful, as information on the chemical composition and elements' binding state can be obtained. In addition to this, it can also be used to determine different phases of amorphous alumina. The binding energy of Al hardly varies (0-0.5 eV) between the different alumina phases. However, oxygen core level binding energies have a larger sensitivity to changing environments and can thus be used for phase identification [24]. If the thin films would contain more than one phase, two or more peaks and also shifting in the peak position can be expected in the O1s photo peak. Figure 2 shows the high resolution XPS spectra of Al2p and O1s core lines of the thin films prepared using EtOH, Pr^iOH and n-BuOH as solvent. All thin films for XPS analysis were coated on Si substrates and heat treated at 500^oC. As seen

in the figure, the peaks of Al2p and O1s are very symmetrical. This suggests only one contribution to the peaks. Table 2 summarises the results of the XPS measurements of the thin films. The peak positions and the symmetry in the O1s core lines of the samples imply that the samples only consist of an aluminium oxide phase. The peak positions and the oxygen/aluminium ratio are consistent with Al_2O_3 [13, 24, 25].

The chemical composition and bonds of the aluminium oxide thin films on double side polished silicon wafer were also analyzed by FT-IR spectroscopy. Figure 3 shows the FT-IR absorption spectra of the thin films before and after heat treatment at 200^{o}C and 500^{o}C, for the three solvents.

Based on the temperature dependency, the spectra can be divided into two parts. The first part consists of the peaks at frequencies higher than 1020 cm^{-1}, and the second part comprises the peaks below 1020 cm^{-1}. As clearly seen in figure 3, after the heat treatment at 200^{o}C the peaks located in the second part give place to two weak and broad peaks.

The broad peak with a maximum at 3620 cm^{-1} in figure 3 is due to the stretching mode of O-H groups [13, 26-29]. This peak disappears after a heat treatment at 500^{o}C. This implies that after a heat treatment at 500^{o}C neither water nor aluminium oxide hydroxide are present in the samples. This result is in line with XPS measurements. The absorption bands between 3000 and 2850 cm^{-1} result from asymmetric and symmetric stretching of aliphatic C-H bonds [25] and they disappear after heat treatment at 200^{o}C as confirmed by TGA curves (figure 1). Two intense absorption peaks located between 1650 and 1500 cm^{-1} are assigned to C=O stretching vibration of acetylacetone and acetic acid [13, 30, 31]. There may be a contribution of the H_2O rocking vibration at 1600 cm^{-1} to the spectra. The peaks between 1500 and 1320 cm^{-1} are assigned to a mixture of C-H bending coming from carbon-hydrogen bonds in the CH_2 and CH_3 groups. C-H wagging and twisting vibrations occur at 1290 cm^{-1}. The peaks between 1200 and 1120 cm^{-1} are assigned to various C-C band vibrations. Two peaks between 1120 and 1020 cm^{-1} are identified as C-O stretching bands. The broad bands located at lower frequency region (between 1000 and 400 cm^{-1}) are related to aluminium oxide [4, 32-34]. When the samples were heated at 200^{o}C, the shape of these bands changed due to the formation of aluminium oxide or oxide hydroxide from aluminium hydroxide. In alumina, aluminium can occupy three different geometries with oxygen which are octahedral (AlO_6), pentahedral (AlO_5) (amorphous structure) and

tetrahedral (AlO_4). When aluminium ions have octahedral coordination (AlO_6), the Al-O stretching and bending modes are seen in the region 500-750cm^{-1} and 350-450 cm^{-1}, respectively. If they have tetrahedral symmetry (AlO_4), the Al-O stretching and bending modes appear in the narrow range 750-850 cm^{-1} and 250-320 cm^{-1}, respectively. The transition alumina phases consist of octahedral (AlO_6) and tetrahedral (AlO_4) aluminium ions [4, 32, 33]. The broad and smooth absorption band without any fine structure in the wave number range from 500 - 900 cm^{-1} characterizes the amorphous aluminium oxide [34]. As seen in figure 3, although the samples prepared with EtOH and n-BuOH after annealing at 500^oC contain both octahedral (AlO_6) and tetrahedral (AlO_4) aluminium ions, in the sample prepared with Pr^iOH after annealing at 500^oC the amorphous structure is dominant. Note that the apparent negative absorption peak at 1110 cm^{-1} is due to a difference in interstitial oxygen concentration in the Czochralski-grown Si substrates [35]. The reduction of interstitial oxygen might be explained by the formation of oxygen thermal donors [36] due to the heat treatments.

Optical constants and thicknesses of a number of films were determined via spectroscopic ellipsometry. Fitting quality is determined by a comparison between model-generated curves and experimental data and for all samples the model fit curves have an excellent agreement with the experimental curves. The mean squared error (MSE) quantifies the difference between model and experimental curves. Although a small MSE is necessary, it is not sufficient to decide the proposed model is correct. To determine the best model in addition to knowledge about the sample, physical laws should be considered. Otherwise a fitting with a small MSE without physical significance can be easily obtained. Cauchy dispersion model results in a good fitting in the transparent region of many materials [37]. Because of transparency of aluminium oxide from UV to IR [1-3], the Cauchy dispersion model was used to calculate the optical constants. The optical model included surface roughness; however, it was found to be lower than 12 nm for all samples. Fitting was performed between 250 nm and 1700 nm, using Complete Ease software (Woollam Inc.). Porosity of the films was calculated using Bruggeman effective medium approximation (EMA) [21]. Reference data such as Cauchy coefficients and refractive index for aluminium oxide were supplied from literature [38].

Table 2 summarizes the results from the spectroscopic ellipsometry analysis on aluminium oxide thin films. The effect of the solvent on the film properties was studied by preparing thin films with different solvent but using

the same conditions. When the samples heat treated at 450^{o}C are compared (A, B and C and G, H, and I), changing alcohol from Pr^{i}OH to EtOH and n-BuOH decreases the thickness of film by 16% and 33%, respectively. When D, E, and F (heat treated at 650^{o}C) are compared, changing alcohol from Pr^{i}OH to EtOH and n-BuOH results in a decrease of 36% and 32%, respectively. Because of the different sizes, polarities and also evaporation rates of the solvents, they present different behaviours during hydrolysis and condensation. Although substitution of the alcohols has an effect on the thickness, it does not have noteworthy effect on the porosity and consequently also the refractive index. Increasing the heating temperature from 450^{o}C to 650^{o}C results in a significant decrease of the thickness of the film prepared with EtOH and a small increase of the porosity in all samples. A decrease in the film thickness with an increase in heating temperature can be expected due to the densification of the film. Because of dehydroxylation during the heat treatment, removing OH groups leave behind pores in the film and an increase in the porosity has been observed. The effect of the spin speed on thickness and refractive index was also investigated (e.g., A, B, C and G, H, I). When the spin speed is increased, a thinner film is obtained with the same refractive index.

The surface properties of the films were investigated via SEM and the films prepared with the three solvents had similar surface properties, all of them homogeneous and crack free. As an example, SEM images of the thin film prepared with ethanol and spin coated at 2000 rpm then heat treated at 500^{o}C is presented in figure 4.

Conclusions

In this work, alumina solutions without any precipitation were successfully synthesized with three alcohols using a non-aqueous sol-gel technique. Although all solutions were stable for at least 1 month, the most stable solution was obtained using n-BuOH. Aluminium oxide thin films prepared using these three solutions were amorphous, crack free and have similar properties. After heat treatment of films at 500^{o}C, only amorphous aluminium oxide films were obtained. Different film thicknesses from 50 to 160 nm with the same refractive index can be obtained by changing the preparation parameters spin speed and solvent. Aluminium oxides synthesized via this method were successfully used as a protection layer for moisture sensitive particles such as sulfides [20].

Acknowledgments

This research is supported by the Interuniversity attraction poles programme IAP/VI-17 (INANOMAT) financed by the Belgian State, Federal science policy office. We gratefully acknowledge Nico De Roo for help with XPS measurements and Jonas Feys for help with TGA/DTA measurements.

References

1. N. Avci, J. Musschoot, P. F. Smet, K. Korthout, A. Avci, C. Detavernier, and D. and Poelman (2009) J. Electrochem. Soc. 156:J333-J337
2. D. Jiang, D. M. Hulbert, U. Anselmi-Tamburini, T. Ng, D. Land, and A. K. Mukherjee (2008) J. Am. Ceram. Soc. 91:151-154
3. E. D. Palik (1998) Handbook of Optical Constants of Solids, Vol. 3, Academic Press, San Diego
4. A.Boumaza, L. Favaro, J. Le´dion, G. Sattonnay, J. B. Brubach, P. Berthet, A. M. Huntz, P. Roy, R. Tétot (2009) J. Solid State Chem. 182: 1171–1176
5. W. M. Zeng, L. Gao, L. H. Gui, and J. K. Guo (1999) Ceram. Int. 25:723-726
6. K. Vanbesien, P. De Visschere, P. F. Smet, and D. Poelman (2006) Thin Solid Films 514:323-328
7. G. Hirata, N. Perea, M. Tejeda, J. A. Gonzalez-Ortega, and J. McKittrick (2005) Opt. Mater. 27:1311-1315
8. K. Tadanaga, N. Katata, and T. Minami (1997) J. Am. Ceram. Soc. 80:1040-1042
9. J. W. Lee, C. W. Won, B. S. Chun, and H. Y. Sohn (1993) J. Mater. Res. 8:3151-3157
10. B. Dong, T. Yang, and M. K. Lei (2007) Sens. Actuators B: Chem. 123:667-670
11. D. W. Thompson, P. G. Snyder, L. Castro, L. Yan, P. Kaipa, and J. A. Woollam (2005) J. Appl. Phys. 97:113511
12. C. F. Guo, B. L. Chu, and Q. Su (2004) Appl. Surf. Sci. 225:198-203
13. N. Ozer, J. P. Cronin, Y. J. Yao, and A. P. Tomsia (1999) Sol. Energy Mater. Sol. Cells 59:355-366

14. E. Langereis, M. Creatore, S. B. S. Heil, M. C. M. Van de Sanden, and W. M. M. Kessels (2006) Appl. Phys. Lett. 89:081915
15. M. D. Groner, S. M. George, R. S. McLean, and P. F. Carcia (2006) Appl. Phys. Lett. 88:051907
16. B. M. Henry, A. G. Erlat, A. McGuigan, C. R. M. Grovenor, G. A. D. Briggs, Y. Tsukahara, T. Miyamoto, N. Noguchi, and T. Niijima (2001) Thin Solid Films 382:194-201
17. X. F. Duan, N. H. Tran, N. K. Roberts, and R. N. Lamb (2009) Thin Solid Films 517:6726-6730
18. F. Di Fonzo, D. Tonini, A. L. Bassi, C. S. Casari, M. G. Beghi, C. E. Bottani, D. Gastaldi, P. Vena, and R. Contro (2008) Appl. Phys. A: Mater. Sci. Process. 93:765-769
19. P. F. Smet, I. Moreels, Z. Hens, and D. Poelman (2010) Materials 3:2834-2883
20. N. Avci, I. Cimieri, P. F. Smet, and D. Poelman, Opt. Mater. Doi:10.1016/j.optmat.2010.07.021
21. A. C. Galca, E. S. Kooij, H. Wormeester, C. Salm, V. Leca, J. H. Rector, and B. Poelsema (2003) J. Appl. Phys. 94:4296-4305
22. N. Avci, P. F. Smet, H. Poelman, N. Van de Velde, K. De Buysser, I. Van Driessche, and D. Poelman (2009) J. Sol-Gel Sci. Technol. 52:424-431
23. M. E. Mata-Zamora and J. M. Saniger (2005) Revista Mexicana De Fisica 51:502-509
24. J. T. Kloprogge, L. V. Duong, B. J. Wood, R. L. Frost (2006) J. Colloid Interface Sci. 296:572-576
25. J. Q. Wang, S. R. Yang, M. Chen, and Q. J. Xue (2004) Surf. Coat. Technol. 176:229-235
26. A. Boumaza, L. Favaro, J. Ledion, G. Sattonnay, J. B. Brubach, P. Berthet, A. M. Huntz, P. Roy, and R. Tetot (2009) J. Solid State Chem. 182:1171-1176
27. C. Morterra and G. Magnacca (1996) Catal. Today 27:497-532
28. M. Nguefack, A. F. Popa, S. Rossignol, and C. Kappenstein (2003) Phys. Chem. Chem. Phys. 5:4279-4289
29. G. Liu, M. J. Jia, Z. Zhou, L. Wang, W. X. Zhang, and D. Z. Jiang (2006) J. Colloid Interface Sci. 302:278-286
30. S. Fessi and A. Ghorbel (2000) J. Sol-Gel Sci. Technol. 19:417-420
31. T. I. Kiyoharu Tadanaga, Noboru Tohge and Tsutomu Minami (1994) J. Sol-Gel Sci. Technol 3:5-10
32. R. Rinaldi, U. Schuchardt (2005) J. Catal. 236: 335-345
33. G. K. Priya, P. Padmaja, K. G. K. Warrier, A. D. Damodaran, G. Aruldhas (1997) J. Mater. Sci. Lett. 16: 1584-1587

34. C. H. Shek, J. K. L. Lai, T. S. Gu, and G. M. Lin (1997) Nanostruct. Mater. 8:605-610

35. University of Reading http://www.reading.ac.uk/infrared/library/infraredmaterials/ir-infraredmaterials-si.aspx Accessed 01 Apr 2011

36. P. Wagner, J. Hage (1989) Appl. Phys. A: Mater. Sci. Process. 49:123-138

37. D. Poelman and P. F. Smet (2003) J. Phys. D: Appl. Phys. 36:1850-1857

38. T. Lichtenstein (1972) Handbook of Thin Film Materials, Academic Press, New York

Figure captions

Fig. 1 TGA/DTA of aluminium oxide sols synthesized with EtOH **(a)**, $Pr^{i}OH$ **(b)**, and n-BuOH (**c)** with a heating rate of $10^{o}C$/min in an air flow.

Fig. 2 XPS spectra of Al and O in aluminium oxide thin films prepared with EtOH **(a)**, $Pr^{i}OH$ (b) and n-BuOH **(c)** after heat treatment at $500^{o}C$.

Fig. 3 FT-IR absorption spectra of aluminium oxide films prepared with EtOH **(a)**, $Pr^{i}OH$ **(b)** and n-BuOH **(c)** before and after heat treatment at $200^{o}C$ and $500^{o}C$. For clarity, the spectra of the samples annealed at $200^{o}C$ and $500^{o}C$ are offset vertically.

Fig. 4 SEM image of an aluminium oxide thin film prepared with EtOH and heat treated at 500°C. (a) and (b) top view of the sample, (c) cross-section of the sample, observed at a grazing angle of 15.

Table captions

Table 1 XPS results of aluminium oxide films heat treated at 500°C.

Table 2 Spectroscopic ellipsometry results of aluminium oxide films.

Tables

Table 1			
Film	Al2p (eV)	O1s(eV)	Ratio O:Al
Prepared with EtOH	74.2	530.7	1.46
Prepared with $Pr^{i}OH$	74.2	531.2	1.50
Prepared with n-BuOH	74.3	530.9	1.53

Table 2							
Sample	Solvent	Spin Speed (rpm)	Heating Temperature (^{o}C)	Thickness (nm)	n @ 632.8nm	Porosity (%)	MSE
A	EtOH	4000	450	69	1.56	26%	6.80
B	$Pr^{i}OH$	4000	450	82	1.55	27%	8.99
C	n-BuOH	4000	450	55	1.57	25%	7.20
D	EtOH	4000	650	48	1.54	28%	4.87
E	$Pr^{i}OH$	4000	650	75	1.54	29%	10.55
F	n-BuOH	4000	650	51	1.54	29%	5.05
G	EtOH	6000	450	59	1.58	24%	6.43
H	$Pr^{i}OH$	6000	450	70	1.57	25%	7.83
I	n-BuOH	6000	450	47	1.60	22%	7.10

Figure 1

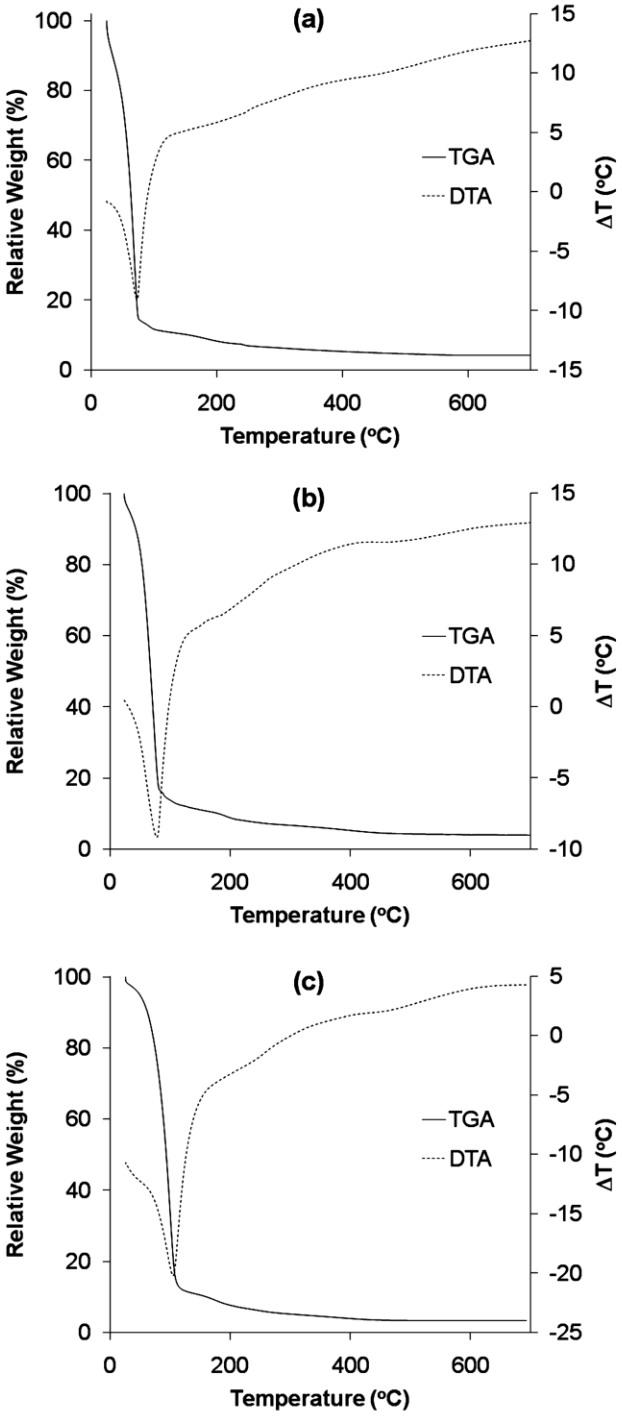
(a)
Relative Weight (%)
ΔT (°C)
TGA
DTA
Temperature (°C)
(b)
Relative Weight (%)
ΔT (°C)
TGA
DTA
Temperature (°C)
(c)
Relative Weight (%)
ΔT (°C)
TGA
DTA
Temperature (°C)

Figure 2

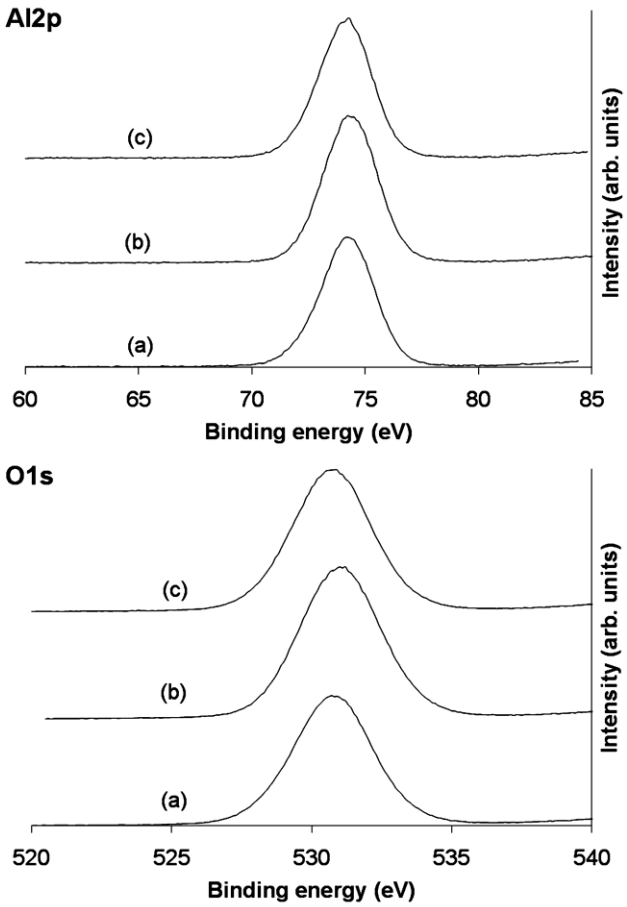
Al2p
(c)
(b)
(a)
Intensity (arb. units)
60
65
70
75
80
85
Binding energy (eV)
O1s
(c)
(b)
(a)
Intensity (arb. units)
520
525
530
535
540
Binding energy (eV)

Figure 3

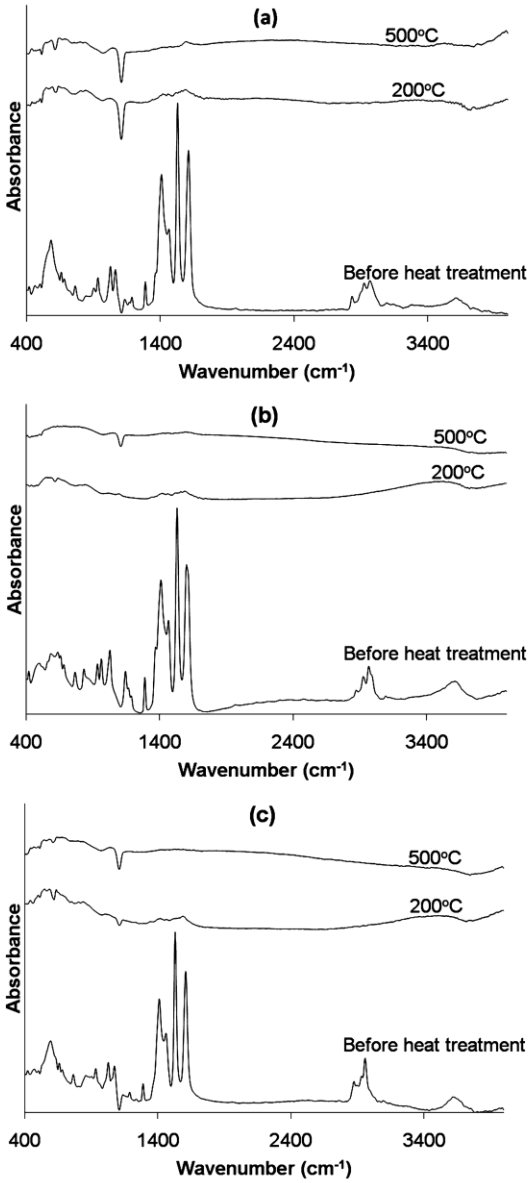
(a)
500°C
200°C
Absorbance
Before heat treatment
400
1400
2400
3400
Wavenumber (cm-1)
(b)
500°C
200°C
Absorbance
Before heat treatment
400
1400
2400
3400
Wavenumber (cm-1)
(c)
500°C
200°C
Absorbance
Before heat treatment
400
1400
2400
3400
Wavenumber (cm-1)

Figure 4